

# Glacial cycle ice-sheet evolution controlled by ocean bed properties

C. Schannwell<sup>1\*</sup>, R. Drews<sup>1</sup>, T.A. Ehlers<sup>1</sup>, O. Eisen<sup>2,3</sup>, C. Mayer<sup>4</sup>, M. Malinen<sup>5</sup>,  
E.C. Smith<sup>2</sup>, and H. Eisermann<sup>2</sup>

<sup>1</sup>Department of Geosciences, University of Tübingen, Tübingen, Germany

<sup>2</sup>Glaciology, Alfred Wegener Institute, Helmholtz Centre for Polar and Marine Research, Bremerhaven,  
Germany

<sup>3</sup>Department of Geosciences, University of Bremen, Bremen, Germany

<sup>4</sup>Bavarian Academy for Sciences and Humanities, Munich, Germany

<sup>5</sup>CSC-IT Center for Science Ltd., Espoo, Finland

## Key Points:

- Ocean bed properties exert a critical control on ice-sheet geometry over full glacial cycle
- Ice thickness and grounding-line position differ by up to 1000 m and 50 km between hard-bed and soft-bed simulations
- Ice-sheet change is characterized by short periods of advance or retreat followed by long periods of ice-sheet stability

---

\*Now at: Max Planck Institute for Meteorology, Bundesstraße 53, 20146 Hamburg, Germany

Corresponding author: Clemens Schannwell, [Clemens.Schannwell@mpimet.mpg.de](mailto:Clemens.Schannwell@mpimet.mpg.de)

## Abstract

Improving constraints on the basal ice/bed properties is essential for accurate prediction of ice-sheet grounding-line positions and stability. Furthermore, the history of grounding-line positions since the Last Glacial Maximum has proven challenging to understand due to uncertainties in bed conditions. Here we use a 3D full-Stokes ice-sheet model to investigate the effect of differing ocean bed properties on ice-sheet advance and retreat over a glacial cycle. We do this for the Ekström Ice Shelf catchment, East Antarctica. We find that predicted ice volumes differ by  $>50\%$ , resulting in two entirely different catchment geometries triggered exclusively by variable ocean bed properties. Grounding-line positions between simulations differ by  $>100\%$  (49 km), show significant hysteresis, and migrate non-steadily with long quiescent phases disrupted by leaps of rapid migration. These results highlight that constraints for both bathymetry and substrate geologic properties are urgently needed for predicting ice-sheet evolution and sea-level change.

## Plain Language Summary

The Antarctic ice sheet is completely surrounded by oceans. However, what type of rock is at the bottom of these oceans is poorly known. During previous glaciations the ice sheet has advanced and retreated multiple times over areas of contemporary oceans. As the ice comes into contact with the ocean floor, friction between ice and ocean floor determines how fast the ice flows and influences the ice-sheet size and shape. Here we present computer simulations of the Ekström Ice Shelf, East Antarctica, that show the importance of the type of rock at the bottom of contemporary oceans for ice sheet advance and retreat. Our simulations reveal that different materials could result in a 50% volume difference. Even though Ekström Ice Shelf is relatively small, there is evidence that similar conditions are present over large areas surrounding the Antarctic ice sheet. This means that the Antarctic ice sheet might have looked very different during past glaciations than previously thought.

## 1 Introduction

Shortcomings in the description of ice dynamics have been recognized as a major limitation for projecting the evolution of the Greenland and Antarctic ice sheets (IPCC AR5, Pachauri et al., 2014). If present sea-level rise rates continue unabated, up to 630 million people will be at annual flood risk by 2100 (Kulp & Strauss, 2019), making improved ice-sheet model projections a priority of high socioeconomic impact. The current state-of-the art for long-term ( $>1,000$  year) ice-sheet simulations requires simplifications in the ice-dynamical equations that result in two limitations. First, it is questionable whether the transition zone between grounded and floating ice (e.g. the grounding zone) is adequately represented in existing long-term simulations (Schoof, 2007). Second, the omission of membrane and bridging stress gradients hamper disentangling the relative contributions of basal sliding and ice deformation to the column averaged ice discharge (MacGregor et al., 2016; Bons et al., 2018). The former is one of the main uncertainties for projecting the sea-level contribution of contemporary ice sheets (Durand et al., 2009; Pattyn & Durand, 2013). The latter is a bottleneck for the inclusion of basal processes such as erosion and deposition of sediments which critically depend on the magnitude of basal sliding (e.g., Humphrey & Raymond, 1994; Egholm et al., 2011; Herman et al., 2011; Yanites & Ehlers, 2016; Alley et al., 2019) and may govern the formation and decay of ice streams (Spagnolo et al., 2016).

Recently, a number of simplified model variants of the full ice-flow equations have been successfully applied to sea-level rise projections using ensemble simula-

68 tions that account for uncertainties in atmospheric and oceanic boundary conditions  
69 over timescales of  $>1,000$  years (e.g., Golledge et al., 2012; Briggs et al., 2014; Pol-  
70 lard et al., 2016). More realistic full-Stokes simulations, on the other hand, have  
71 thus far only been applied to a maximum of 1,000 years for real-world geometries  
72 due to the high computational demands, both, in terms of mesh resolution and the  
73 physics required to solve for a freely evolving grounding line (Gillet-Chaulet et al.,  
74 2012; Seddik et al., 2012; Favier et al., 2014; Schannwell et al., 2019).

75 A particular challenge that arises in model simulations over long time scales  
76 ( $\geq 40,000$  years) is that the ice sheet advances and retreats over ocean beds where  
77 bathymetry and its geological properties are often poorly known. While the slopes  
78 of the ice-shelf cavity and the bed topography farther upstream have received much  
79 attention because of their control on ice-sheet stability (e.g., Schoof, 2007; Tsai et  
80 al., 2015), comparatively little research has focused on the corresponding geologi-  
81 cal properties controlling basal sliding or the lack thereof. Estimating basal friction  
82 parameters under contemporary ice sheets (e.g. basal friction between the ice sheet  
83 and the underlying substrate) is virtually impossible by direct measurements and  
84 can only be inferred indirectly on a continental scale by solving an optimization  
85 problem matching today's surface velocities and/or ice thickness (e.g., MacAyeal,  
86 1993; Gillet-Chaulet et al., 2012; Cornford et al., 2015). Furthermore, the inferred  
87 basal friction coefficient is often spatially heterogeneous and can vary by up to  
88 five orders of magnitude under the present-day Antarctic ice sheet (Cornford et  
89 al., 2015). To what extent this variability truly reflects variability in geology, or is  
90 falsely introduced by the approximations in the ice-dynamical equations or omission  
91 of ice anisotropy is unknown. Even less is known about the properties of ocean beds  
92 under contemporary ice shelves. In previous sensitivity studies, basal properties of  
93 ocean beds have been identified as a major source of uncertainty in ice-dynamic  
94 models (e.g., Pollard & DeConto, 2009; Pollard et al., 2016; Albrecht et al., 2019).  
95 However, the lack of a comprehensive Antarctic-wide distribution map of sedimen-  
96 tary deposits and crystalline rock, together with the absence of a full-Stokes model  
97 over the time scales required, leaves characterization of basal friction parameters and  
98 their consequences for ice-sheet growth and decay poorly constrained.

99 Here we employ a three-dimensional (3D), isotropic, thermomechanically-  
100 coupled full-Stokes model (Elmer/Ice, Gagliardini et al. (2013)) to narrow the time  
101 gap between projections from simplified model simulations over long timescales, and  
102 ice-dynamically more complete simulations over shorter time scales. We do this with  
103 a highly parallelized numerical scheme allowing to maintain a high mesh resolution  
104 ( $\sim 1$  km) and a freely evolving grounding line over glacial/interglacial timescales.  
105 Our simulations focus on the effect of ocean bed properties seawards of today's  
106 grounding line and to quantify their impact on the evolution of the entire catch-  
107 ment. This is done for the Ekström Ice Shelf catchment, Dronning Maud Land, East  
108 Antarctica (Fig. 1), containing multiple ice rises and pinning points (Schannwell et  
109 al., 2019; Drews et al., 2013), and hosting Neumayer Station III. Uncertainties in  
110 the contemporary ice-sheet geometry are minimal because of previous dense airborne  
111 radar surveys in the vicinity of Neumayer Station III (Fretwell et al., 2013). Unlike  
112 many other ice shelves, the bathymetry in this area is known to a high accuracy,  
113 across much of the sub-ice-shelf, from extensive seismic reflection surveying (Smith  
114 et al., 2019). This has been extended to cover the whole cavity by aero-gravimetry  
115 measurements (H. Eisermann 2019, personal communication). Furthermore, there  
116 is evidence in this area from multiple geophysical observations about contrasting  
117 ocean bed properties (Kristoffersen et al., 2014). While much recent research has  
118 focused on the fast flowing outlet glaciers of Antarctica, we stress the importance of  
119 also studying catchments characterised by slower moving ice ( $< 300$  m/yr), as they  
120 occupy  $\sim 90\%$  of the contemporary Antarctic grounding line and account for 30% of  
121 the total ice discharge (see SI, sec. 5; Bindshadler et al., 2011; Rignot et al., 2011).

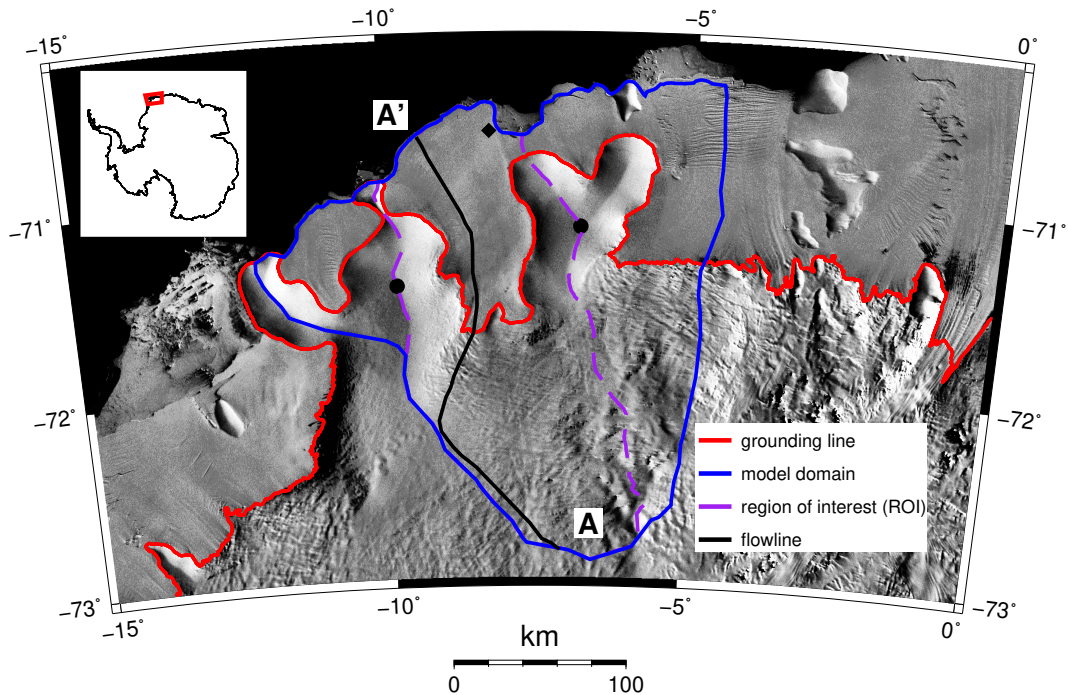


**Figure 1.** Overview of the Ekström Ice Shelf catchment with present-day grounding line and model domain. Black square shows location of Neumayer Station III. Filled black circles indicate location of ice rises. Flowline (A-A') is shown in Fig. 4.

122 The results we obtain for the Ekström Ice Shelf catchment are therefore relevant for  
 123 many other catchments around Antarctica and hence the total budget.

## 124 2 Materials and Methods

### 125 2.1 Ice sheet model and external forcing

126 We use the transient, thermomechanically-coupled full-Stokes model Elmer/Ice  
 127 (Gagliardini et al., 2013). The finite element model solves the full ice-flow equations  
 128 in 3D for ice deformation and incorporates a freely evolving grounding line without  
 129 parameterizations. The equations are solved on a model grid that has a background  
 130 resolution of 6 km, and is locally refined down to 1 km at today's grounding line and  
 131 seaward of today's grounding line at the Ekström Ice Shelf. Subglacial topography is  
 132 taken from Bedmap2 (Fretwell et al., 2013) for the grounded ice sheet, but updated  
 133 for the bathymetry underneath Ekström Ice Shelf based on recent seismic surveys  
 134 and aero-gravimetry (H. Eisermann 2019, personal communication). Underneath ice  
 135 shelves outside the area of interest, the Bedmap2 bathymetry is lowered by  $\sim 300$  m  
 136 to ensure that the ice shelf is floating, as Bedmap2 is unrealistically shallow. Our  
 137 present day surface elevation is a merged product of CryoSat-2 and, where avail-  
 138 able, higher-resolution TanDEM-X digital elevation models (Schannwell et al., 2019).  
 139 Ice temperature is initialized to a steady state for present-day conditions (see SI,  
 140 sec. 2.4; Zhao et al., 2018; Rückamp et al., 2018). The temperature model is forced  
 141 at the ice surface by a present-day temperature distribution (Comiso, 2000) plus a  
 142 temporal surface temperature change that is derived from the nearby EDML ice core  
 143 (Graf et al., 2002), located some 700 km to the south-east of the region of interest  
 144 (ROI; Fig. 1) on the Antarctic plateau. At the grounded basal boundary, a spatially

variable but time-invariant heat flux is prescribed (Martos et al., 2017), while ice temperature is set to the pressure-melting-point at the bottom of floating ice. The surface mass balance (SMB) parameterization follows Ritz et al. (2001). We apply a present-day SMB field (Lenaerts et al., 2014). Temporal change in the SMB is proportional to the exponential of surface temperature change (see SI, sec. 2.3.2). The basal mass balance (BMB) applied at the ice-shelf underside is proportional to the square of the temperature difference between the ice-shelf underside and the ocean temperature at the continental shelf edge (Beckmann & Goosse, 2003). Ocean temperature variations are a damped ( $\sim 40\%$ ) and delayed ( $\sim 3,000$  years) version of the surface temperature variation (Bintanja et al., 2005). Sea level is varied according to Lambeck et al. (2014) which includes isostatic and tectonic contributions. Underneath the grounded ice sheet, we apply a linear Weertman-type sliding law.

## 2.2 Experimental design

We investigate ice-sheet growth and decay over 40,000 years. During the first 20,000 years the atmospheric and oceanic forcing simulates the transition from an interglacial to a glacial (henceforth called the advance phase). We then symmetrically reverse the climate forcing to simulate deglaciation (henceforth called the retreat phase). The symmetrical reversal of the model forcing enables investigation of hysteresis effects. The interglacial starting conditions are chosen with present day properties and characteristics, so that the best possible basal friction coefficient beneath the grounded ice sheet can be found using today's ice-sheet geometry and surface velocities (Schannwell et al., 2019). The glacial conditions are chosen to resemble the Last Glacial Maximum for which we have good constraints for atmospheric forcing from the nearby EDML ice core. We consider two end-member basal-property scenarios by prescribing either soft ocean bed conditions (mimicking sediment deposits) or hard ocean bed conditions (mimicking crystalline rock) for all present-day ocean cavities in the modelling domain. The tested end-member scenarios of basal traction coefficients encompasses what other ice-sheet models have inferred (e.g., Cornford et al., 2015) for the grounded portion underneath the present-day Antarctic ice sheet (basal traction coefficient ranging from  $10^{-1}$  MPa  $\text{m}^{-1}$  yr for sediments to  $10^{-5}$  MPa  $\text{m}^{-1}$  yr for crystalline bedrock). This means that simulated differences in ice volume and grounding-line position should be interpreted as the maximum envelope of uncertainties resulting from different ocean bed properties. We perform the simulations with a) the standard Elmer/Ice setup using the Multifrontal Massively Parallel Sparse (MUMPS) direct solver for ice velocities; and b) using a stable iterative solver for ice velocities (see SI, sec. 2.6; Malinen et al., 2013), resulting in a total of four simulations.

## 3 Results and Discussion

### 3.1 Influence of bed hardness on ice-sheet growth and decay

The two scenarios of hard vs. soft bed result in two fully different ice sheet geometries at the glacial maximum with different volumes (Fig. 2), fluxes, and grounding line positions through time (Figs. 3 and 4). For example, the simulated hard bed ice sheet is in many areas more than twice as thick as the soft bed ice sheet, with maximum ice thickness differences between hard and soft bed reaching 1,036 m or 120% (Fig. 3). In more detail, the differences between these simulations are as follows:

First, the hard bed ice sheet results in a thick, slow, and large volume ice sheet after 20,000 years at glacial conditions. During the advance phase, volume increases occur step-wise with three distinct periods of volume increases (Fig. 2). These periods of volume increase in the ROI are short ( $< 2000$  years) and are interrupted

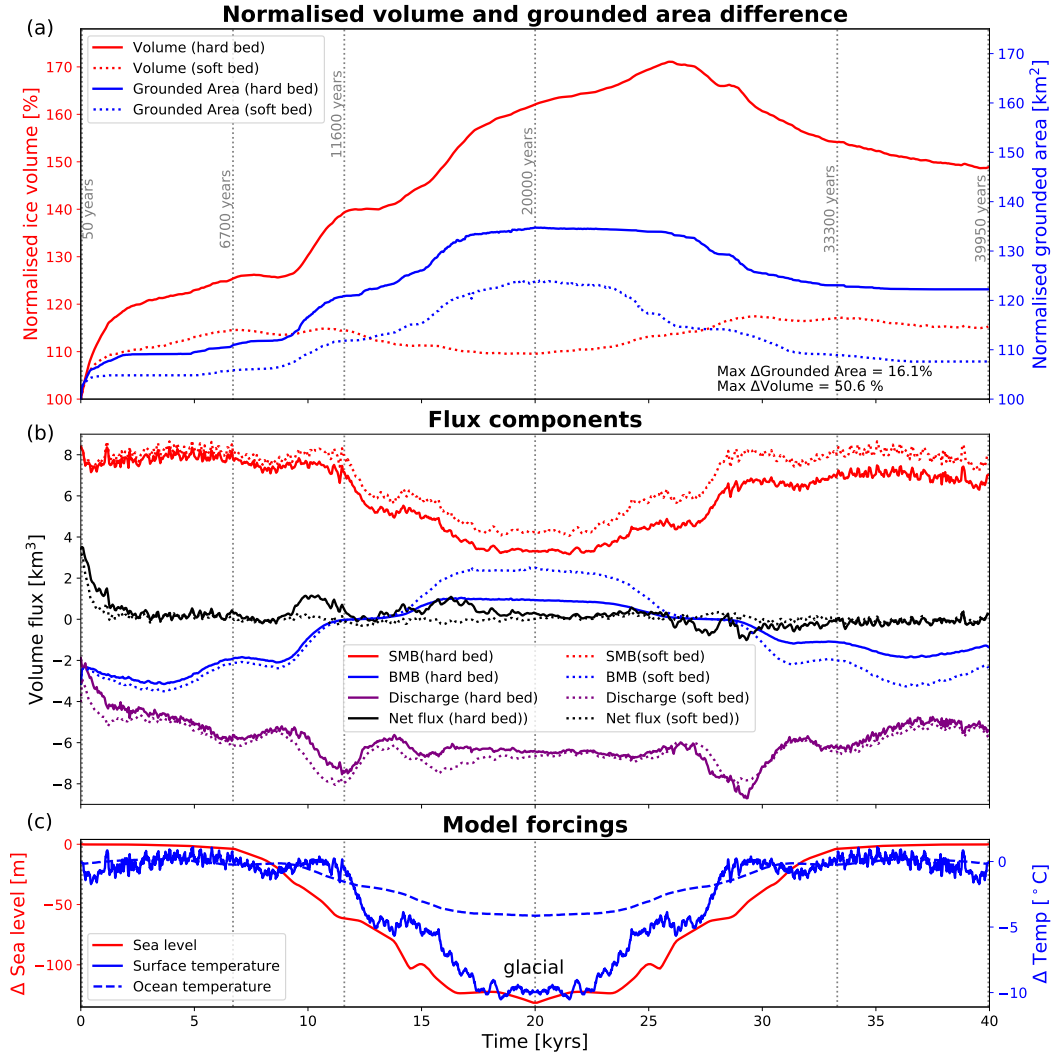


**Figure 2.** Ice-sheet evolution and model forcing for soft and hard-bed simulations. (a) shows volume and grounded area evolution normalised to present-day. (b) shows corresponding mass balance fluxes, and (c) shows most important model forcings. Vertical grey stippled lines show time slices shown in Figs. 3 and 4.

195 by longer periods of little ice volume change. At the glacial maximum, the volume  
 196 increase in comparison to the interglacial is  $\sim 60\%$ . During the first  $\sim 8,000$  years in  
 197 the retreat phase, the hard bed simulation continues to gain volume albeit at a slow  
 198 rate. The continued raising of the sea level finally forces the hard bed ice sheet to  
 199 start losing volume. However, the rate of volume loss is small, such that after a full  
 200 glacial cycle, the total ice volume is still  $\sim 47\%$  more of what is was at the beginning  
 201 of the simulation. This relative stability of the hard-bed ice sheet during the retreat  
 202 phase is a consequence of the higher levels of basal friction provided by the hard  
 203 bed.

204 Second, unlike the hard-bed simulations, the soft-bed simulation leads to a  
 205 thin, fast, and small volume ice sheet at glacial conditions. During the advance  
 206 phase, this simulation does not show a step-wise volume gain pattern. In fact, apart  
 207 from an initial volume gain in the first 1,000 years of the advance phase ( $\sim 10\%$ ),

208 there is very little volume change. This leads to a volume increase of merely  $\sim 8\%$  at  
209 the glacial maximum. The trend of little volume variations continues during the re-  
210 treat phase, where in the first 10,000 years a volume increase of  $\sim 8\%$  occurs, before  
211 the volume remains approximately constant for the remainder of the retreat phase.

212 The entirely different ice-sheet geometries for soft and hard-bed simulations  
213 have consequences for the two ice rises present in the catchment (Fig.1). While both  
214 ice rises and their divide positions are very little affected by the soft bed simula-  
215 tions, they are partly overrun in the hard bed simulation such that their local ice  
216 flow centre vanishes (SI video 1).

217 The predicted differences between the hard-bed and soft-bed simulations un-  
218 derline the high significance of a proper choice of basal properties used for ocean  
219 beds. The higher basal friction in the hard-bed case leads to elevated back stress  
220 and corresponding dynamical thickening of the inland ice sheet far upstream of the  
221 grounding line. Although the SMB and BMB forcings equally depend on the ice-  
222 sheet geometry through the applied parameterizations, these effects are small com-  
223 pared to the ice-dynamically induced thickening (Fig. 3). This clearly shows that  
224 in the absence of other forcing mechanisms, ocean bed properties exert a first-order  
225 control on ice-sheet growth and decay. Geomorphological evidence from underneath  
226 Ekström Ice Shelf indicates that the grounding line was likely near the shelf front  
227 at the LGM (Smith et al., 2019). This observation matches well with our hard-bed  
228 simulations.

229 Owing to the paucity of observational constraints, numerical modelling stud-  
230 ies have often applied a binary distribution of sediment-based ocean beds and  
231 crystalline-based ocean beds (e.g., Pollard & DeConto, 2009; Whitehouse et al.,  
232 2012). Hereby, most of the ocean bed areas surrounding Antarctica are assumed  
233 to be sediment-based. However, geophysical observations in our study area and  
234 elsewhere in Antarctica (e.g., Gohl et al., 2013; Kristoffersen et al., 2014) indicate  
235 a much more heterogeneous substrate distribution of sediment deposits and crys-  
236 talline bedrock on the continental shelf. Some of these crystalline bedrock features  
237 like the Explora Wedge in Dronning Maud Land are more than 1000 km long (Gohl  
238 et al., 2013; Kristoffersen et al., 2014). Based on our simulations, such crystalline  
239 outcrops under ice shelves will have large impacts on ice thickness and ice volume  
240 of the Antarctic ice sheet over the last glacial cycle. The differences in ice volume  
241 and ice thickness between hard and soft bed are such that they may help to explain  
242 the “missing ice” (Clark & Tarasov, 2014) problem at the LGM, if extrapolated to  
243 the Antarctic ice sheet. This problem relates to the fact that current sea-level recon-  
244 structions suggest a sea-level drop of  $\sim 130$  m at the LGM compared to present-day  
245 conditions (Simms et al., 2019). However, reconstructions of all major ice sheets  
246 at the LGM only account for  $\sim 114$  m of sea-level drop, so that  $\sim 16$  m of sea-level  
247 equivalent is unaccounted for.

248 Finally (third), the ramifications of heterogeneous ocean bed properties go  
249 beyond ice volume considerations. Different levels of basal traction strongly affect  
250 the magnitude of basal sliding. This in turn determines how much material is eroded  
251 underneath the ice sheet and transported across the grounding line. As erosion rates  
252 are commonly approximated as basal sliding to some power (e.g., Herman et al.,  
253 2015; Koppes et al., 2015), any differences in basal sliding velocities are exacerbated  
254 when erosion volumes are computed (see SI, sec. 6). This uncertainty in eroded  
255 material produced has implications for how much sediment is available at the ice-  
256 bedrock interface and therefore if it is a hard- vs. soft-bed interface and its temporal  
257 variability.

### 258 3.2 Grounding-line and ice-sheet stability

259 Stable grounding-line positions for both simulations are associated with periods  
 260 of ice-sheet stability (Fig. 2). In our simulations, there are three distinct periods  
 261 of grounding-line stability in the advance phase and one period of grounding-line  
 262 stability in the retreat phase. All of these four periods are longer than 3,000 years.  
 263 Periods of grounding-line advance in comparison are characterized by short leaps  
 264 taking no longer than 1,000-2,000 years (Fig. 2). These stable ice-sheet configura-  
 265 tions are not controlled by a single specific forcing alone, but are due to a combi-  
 266 nation of sea-level forcing, basal traction of the ocean bed, and ocean bathymetry.  
 267 Other forcing mechanisms such as the SMB and BMB are of secondary importance.

268 During the advance phase, differences in grounding-line positions between the  
 269 hard-bed and soft-bed simulations gradually increase from 7 km after  $\sim 1,500$  years  
 270 to over 37 km after 11,600 years, and finally to its maximum difference of 49 km at  
 271 the glacial maximum (Fig. 4). This means that grounding-line advance for the hard  
 272 bed is more than twice as far ( $\sim 110\%$  larger) than its soft bed counterpart in the  
 273 advance phase.

274 In the retreat phase, the soft-bed simulation shows higher grounding-line  
 275 fidelity compared to the hard-bed simulation. The soft bed starts to exhibit  
 276 grounding-line retreat after  $\sim 4,000$  years into the retreat phase, whereas the hard  
 277 bed does not show grounding-line retreat for  $\sim 8,000$  years into the retreat phase.  
 278 This can be attributed to the fact that ice discharge for the soft-bed simulation is  
 279 dominated by basal sliding and higher ice velocities. In comparison, in the hard bed  
 280 simulation ice discharge is dominated by internal deformation and almost no basal  
 281 sliding, resulting in a much thicker ice sheet. This means that more ice needs to be  
 282 removed before the grounded ice can detach from its subglacial material and initiate  
 283 grounding-line motion, thereby resulting in a much slower response time to changes  
 284 in the model forcing.

285 While our employed modelling approach make it unlikely that the timing of  
 286 our modelled stable grounding-line positions are correct, they can still serve as spa-  
 287 tial markers of areas where depositional landforms such as Grounding-Zone Wedges  
 288 (GZWs) may be found. Their height and width can be exploited to estimate the  
 289 erosive power of the upstream catchment at the time of deposition (Batchelor &  
 290 Dowdeswell, 2015). Assuming similar supply of subglacial material to the grounding  
 291 line, the hard-bed case should result in thicker grounding zone wedges, because it  
 292 exhibits longer periods of grounding-line stability. However, if erosion is approxi-  
 293 mated by basal sliding to some power, sediment supply should be much higher for  
 294 the soft-bed simulation (SI Fig. 8), potentially offsetting the effect of higher tem-  
 295 poral grounding-line fluctuation. Our calculations indicate that for current erosion  
 296 laws, this effect could outweigh greater grounding-line stability, but other processes  
 297 such as sediment transport ought to be considered before a definitive assessment can  
 298 be made.

### 299 3.3 Hysteresis of ice-sheet simulations

300 Next we compare the ice-sheet history and results from the advance phase and  
 301 the retreat phase simulations. We focus on the effect of basal properties and their  
 302 impact on ice-sheet hysteresis. After a full glacial cycle in which atmospheric and  
 303 oceanic forcing are essentially symmetrically reversed for the advance and retreat  
 304 phase, both of our simulations show hysteresis because the ice sheet does not return  
 305 to its initial geometry. However, the hysteresis effect is smaller for the soft-bed case  
 306 with the grounding-line being 19 km farther downstream compared to its initial po-  
 307 sition (Fig. 4), resting on the last subglacial topographic high before the retrograde  
 308 sloping topography would cause it to retreat to its initial position. The hysteresis

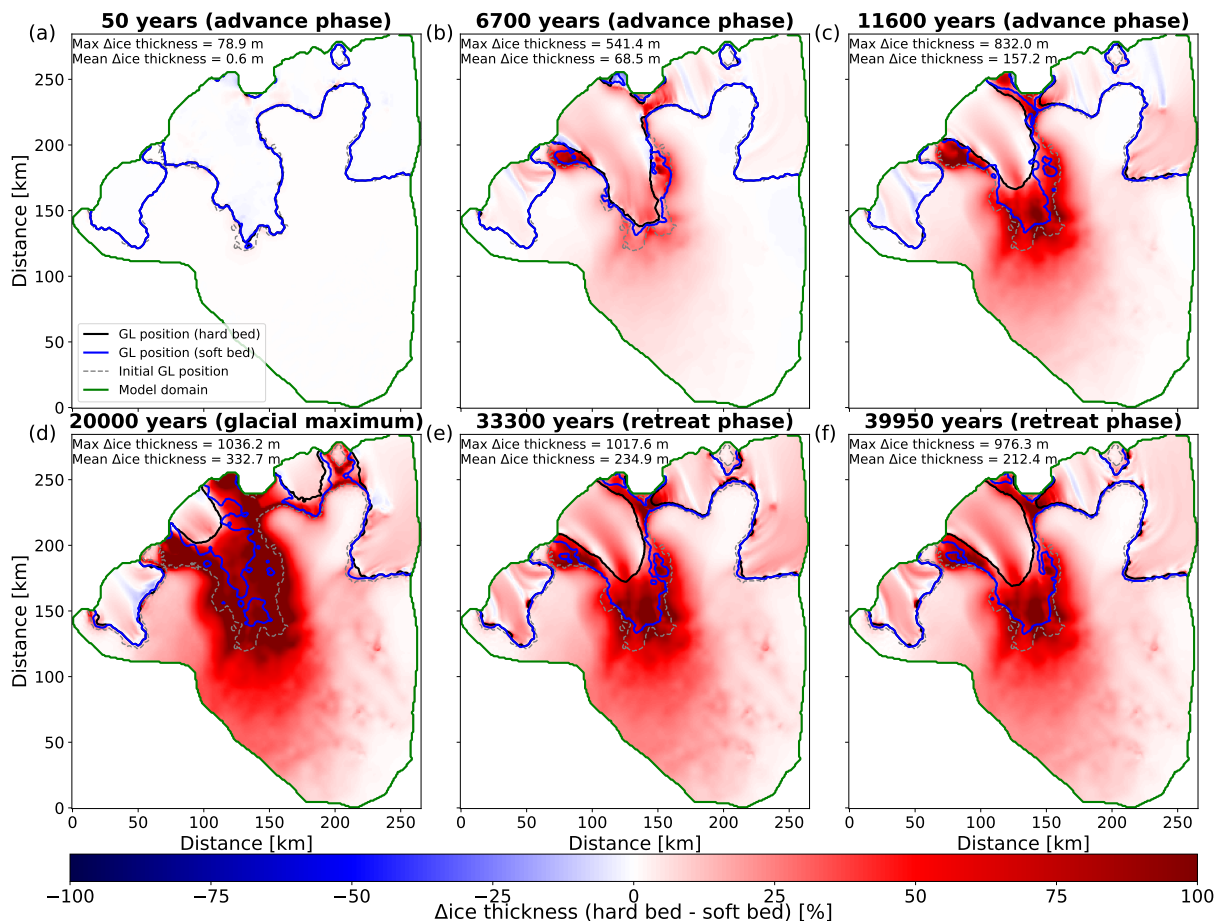


**Figure 3.** Differences in plan-view of ice thickness and grounding-line positions between the hard and soft-bed simulations at selected time slices. (a-d) show differences in the advance phase and (e,f) show differences in the retreat phase.

309 effect is much more pronounced in the hard-bed simulation in which the grounding  
 310 line is 57 km downstream of its initial position (Fig. 4). This means that during the  
 311 retreat phase, the grounding-line retreats only  $\sim 39\%$  in comparison to the simulated  
 312 grounding-line advance during the retreat phase of the hard-bed simulation. Both  
 313 simulations show very little retreat in the last 9,000 years of the retreat phase with  
 314 grounding-line retreat magnitudes  $< 7$  km in this time span. This coincides with  
 315 the period of little sea-level variations, leading us to conclude that at least for the  
 316 retreat phase, sea-level forcing is the most important model forcing.

317 Our results underline the dependence of the final ice-sheet geometry on the  
 318 model's initial state over timescales of a glacial cycle or longer. The modelled hys-  
 319 teresis behavior shows the non-linear response of ice-sheet evolution to very similar  
 320 model forcing, a particularly challenging problem for model simulations over at least  
 321 one advance and retreat cycle (Pollard & DeConto, 2009; Gasson et al., 2016). This  
 322 means that the employed modelling framework will likely not result in the correct  
 323 ice-sheet geometry at the LGM due to non-linear feedback mechanisms such as the  
 324 marine-ice-sheet instability (Schoof, 2007; Durand et al., 2009), the height-mass  
 325 balance feedback (Oerlemans, 2002), and remaining uncertainties regarding the  
 326 subglacial topography.

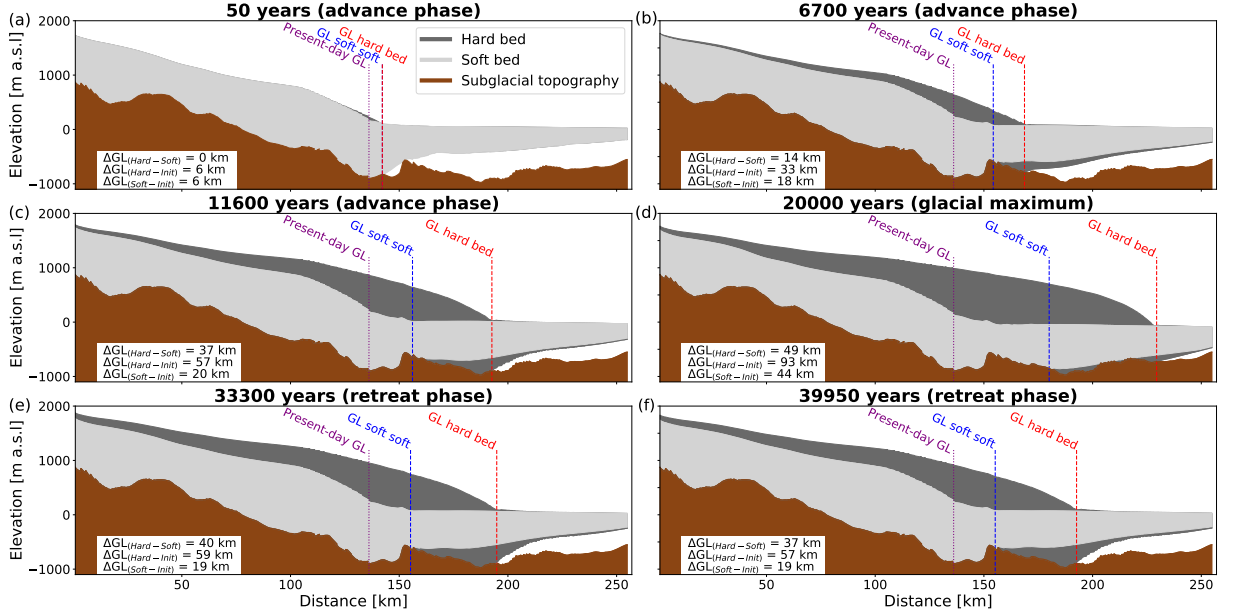


**Figure 4.** Difference in ice-sheet geometry and grounding-line position along a flowline (A-A' in Fig. 1) for the soft and hard-bed simulations. (a-d) show differences in the advance phase and (e,f) show differences in the retreat phase.

327

### 3.4 Model limitations

328

329

330

331

332

333

334

335

336

337

338

339

340

341

The modelling approach presented here is tailored towards capturing ice and grounding-line dynamics to high accuracy at the cost of comparatively naive parameterizations for the SMB and BMB which can be improved in the future. Also, we have not considered glacial isostatic adjustment (GIA). Until recently, GIA was considered to be only important on timescales exceeding 1,000 years. However, recent progress has revealed that due to lower than previously assumed mantle viscosities, response times of GIA to ice unloading can be as short as five years for certain sections in Antarctica (Barletta et al., 2018; Whitehouse et al., 2019). While present-day GIA rates for East Antarctica are relatively low ( $\sim 1\text{mm/yr}$  (Martín-Español et al., 2016)) in comparison to regions of high mass loss in Antarctica, the effect over 20,000 years could amount to  $\sim 20\text{ m}$  of elevation drop for the subglacial topography. This number is small in comparison to for example sea-level variations ( $\sim 130\text{ m}$ ), but may nevertheless result in a grounding-line position that is not as far advanced at the glacial maximum as presented in our simulations.

342

## 4 Conclusions

343

344

345

346

347

348

349

350

351

352

We investigated the effect of basal ocean bed properties on ice-sheet geometry over a full glacial cycle. We find that sediment-covered ‘slippery’ ocean beds result in entirely different ice-sheet geometries, ice-sheet advance and retreat patterns, and grounding-line positions in comparison to crystalline ‘sticky’ ocean beds. Based on our simulations in conjunction with geophysical observations (Smith et al., 2019), we think that substrate distribution (sediments vs. crystalline bedrock) on the continental shelf might be more heterogeneous than previously thought. Recent geomorphological evidence indicates that the grounding line was close to the continental shelf front at the LGM, leading us to conclude that the hard ocean bed simulation matches better with observations than the soft ocean bed simulation.

353 The differences between hard-bed and soft-bed simulations (>50% ice vol-  
 354 ume, >1000 m ice thickness, and >100% grounding line motion) are such that they  
 355 may help to reduce the discrepancy between reconstructed sea-level drop and sea-  
 356 level equivalent stored in all ice sheets at the LGM (“missing ice” problem (Clark  
 357 & Tarasov, 2014)). For example, if we extrapolate our volume difference between  
 358 hard and soft bed (~50%) to the entire ice sheet at the LGM, we could reduce the  
 359 discrepancy by ~33% to ~10 m sea-level equivalent. However, additional studies  
 360 like ours are needed for other locations to establish if our results are more regionally  
 361 valid, or if local conditions within each catchment lead to different results.

362 Owing to our new modelling setup, we reduced computation times in compari-  
 363 son to previous simulations by ~80% and extended the temporal range of full-Stokes  
 364 simulations by a factor of 40 compared to previous studies. Considering the uncer-  
 365 tainties surrounding internal ice dynamics, this provides an important step forward  
 366 to reduce uncertainties and brings us closer to a process-based understanding of a  
 367 number of subglacial processes (e.g. glacial erosion).

### 368 Acknowledgments

369 Clemens Schannwell was supported by the Deutsche Forschungsgemeinschaft (DFG)  
 370 grant EH329/11-1 (to TAE) in the framework of the priority programme “Antarctic  
 371 Research with comparative investigations in Arctic ice areas”. Reinhard Drews was  
 372 funded in the same project under MA 3347/10-1. Reinhard Drews is supported by  
 373 the DFG Emmy Noether grant DR 822/3-1. The authors gratefully acknowledge  
 374 the Gauss Centre for Supercomputing e.V. ([www.gauss-centre.eu](http://www.gauss-centre.eu)) for providing  
 375 computing time on the GCS Supercomputer SuperMUC-NG at Leibniz Super-  
 376 computing Centre ([www.lrz.de](http://www.lrz.de)). The Elmer/Ice code is publicly available through  
 377 GitHub (<https://github.com/ElmerCSC/elmerfem>, lastaccess: 05 November 2019).  
 378 All simulations were performed with version 8.3 (rev. 74a4936). Elmer/Ice scripts  
 379 including all necessary input files to reproduce the simulations are available at  
 380 <https://doi.org/10.5281/zenodo.3564168> (Schannwell (2019), last access: 5 November  
 381 2019).

### 382 References

- 383 Albrecht, T., Winkelmann, R., & Levermann, A. (2019). Glacial cycles simulation of  
 384 the Antarctic Ice Sheet with PISM - Part 2: Parameter ensemble analysis. *The*  
 385 *Cryosphere Discuss.*, 2019, 1–38. doi: 10.5194/tc-2019-70
- 386 Alley, R. B., Cuffey, K. M., & Zoet, L. K. (2019). Glacial erosion: status and out-  
 387 look. *Annals of Glaciology*, 1–13. doi: 10.1017/aog.2019.38
- 388 Barletta, V. R., Bevis, M., Smith, B. E., Wilson, T., Brown, A., Bordoni, A., ...  
 389 Wiens, D. A. (2018). Observed rapid bedrock uplift in Amundsen Sea  
 390 Embayment promotes ice-sheet stability. *Science*, 360(6395), 1335. doi:  
 391 10.1126/science.aao1447
- 392 Batchelor, C., & Dowdeswell, J. (2015). Ice-sheet grounding-zone wedges (GZWs) on  
 393 high-latitude continental margins. *Marine Geology*, 363, 65–92. doi: 10.1016/  
 394 j.margeo.2015.02.001
- 395 Beckmann, A., & Goosse, H. (2003). A parameterization of ice shelf-ocean interac-  
 396 tion for climate models. *Ocean modelling*, 5(2), 157–170.
- 397 Bindschadler, R., Choi, H., Wichlacz, A., Bingham, R., Bohlander, J., Brunt, K., ...  
 398 Young, N. (2011). Getting around Antarctica: new high-resolution mappings  
 399 of the grounded and freely-floating boundaries of the Antarctic ice sheet cre-  
 400 ated for the International Polar Year. *The Cryosphere*, 5(3), 569–588. doi:  
 401 10.5194/tc-5-569-2011
- 402 Bintanja, R., van de Wal, R. S., & Oerlemans, J. (2005). Modelled atmospheric tem-  
 403 peratures and global sea levels over the past million years. *Nature*, 437(7055),

- 404 125–128. doi: 10.1038/nature03975
- 405 Bons, P. D., Kleiner, T., Llorens, M.-G., Prior, D. J., Sachau, T., Weikusat, I., &  
406 Jansen, D. (2018). Greenland Ice Sheet: Higher Nonlinearity of Ice Flow  
407 Significantly Reduces Estimated Basal Motion. *Geophysical Research Letters*,  
408 *45*(13), 6542–6548. doi: 10.1029/2018GL078356
- 409 Briggs, R. D., Pollard, D., & Tarasov, L. (2014). A data-constrained large ensemble  
410 analysis of Antarctic evolution since the Eemian. *Quaternary Science Reviews*,  
411 *103*, 91–115. doi: 10.1016/j.quascirev.2014.09.003
- 412 Clark, P. U., & Tarasov, L. (2014). Closing the sea level budget at the Last Glacial  
413 Maximum. *Proceedings of the National Academy of Sciences*, *111*(45), 15861.  
414 doi: 10.1073/pnas.1418970111
- 415 Comiso, J. C. (2000). Variability and Trends in Antarctic Surface Temperatures  
416 from In Situ and Satellite Infrared Measurements. *Journal of Climate*, *13*(10),  
417 1674–1696. doi: 10.1175/1520-0442(2000)013<1674:VATIAS>2.0.CO;2
- 418 Cornford, S. L., Martin, D. F., Payne, A. J., Ng, E. G., Le Brocq, A. M., Gladstone,  
419 R. M., . . . Vaughan, D. G. (2015). Century-scale simulations of the response  
420 of the West Antarctic Ice Sheet to a warming climate. *The Cryosphere*, *9*(4),  
421 1579–1600. doi: 10.5194/tc-9-1579-2015
- 422 Drews, R., Martín, C., Steinhage, D., & Eisen, O. (2013). Characterizing the glacio-  
423 logical conditions at Halvfarryggen ice dome, Dronning Maud Land, Antarc-  
424 tica. *Journal of Glaciology*, *59*(213), 9–20. doi: 10.3189/2013JoG12J134
- 425 Durand, G., Gagliardini, O., de Fleurian, B., Zwinger, T., & Le Meur, E. (2009).  
426 Marine ice sheet dynamics: Hysteresis and neutral equilibrium. *Journal of*  
427 *Geophysical Research*, *114*(F3). doi: 10.1029/2008JF001170
- 428 Egholm, D. L., Knudsen, M. F., Clark, C. D., & Lesemann, J. E. (2011). Modeling  
429 the flow of glaciers in steep terrains: The integrated second-order shallow ice  
430 approximation (iSOSIA). *Journal of Geophysical Research*, *116*(F2). doi:  
431 10.1029/2010JF001900
- 432 Favier, L., Durand, G., Cornford, S. L., Gudmundsson, G. H., Gagliardini, O.,  
433 Gillet-Chaulet, F., . . . Le Brocq, A. M. (2014). Retreat of Pine Island Glacier  
434 controlled by marine ice-sheet instability. *Nature Climate Change*, *4*, 117.
- 435 Fretwell, P., Pritchard, H. D., Vaughan, D. G., Bamber, J. L., Barrand, N. E.,  
436 Bell, R., . . . Zirizzotti, A. (2013). Bedmap2: improved ice bed, surface  
437 and thickness datasets for Antarctica. *The Cryosphere*, *7*(1), 375–393. doi:  
438 10.5194/tc-7-375-2013
- 439 Gagliardini, O., Zwinger, T., Gillet-Chaulet, F., Durand, G., Favier, L., de Fleurian,  
440 B., . . . Thies, J. (2013). Capabilities and performance of Elmer/Ice, a  
441 new-generation ice sheet model. *Geosci. Model Dev.*, *6*(4), 1299–1318. doi:  
442 10.5194/gmd-6-1299-2013
- 443 Gasson, E., DeConto, R. M., Pollard, D., & Levy, R. H. (2016). Dynamic Antarc-  
444 tic ice sheet during the early to mid-Miocene. *Proceedings of the National*  
445 *Academy of Sciences*, *113*(13), 3459. doi: 10.1073/pnas.1516130113
- 446 Gillet-Chaulet, F., Gagliardini, O., Seddik, H., Nodet, M., Durand, G., Ritz, C.,  
447 . . . Vaughan, D. G. (2012). Greenland ice sheet contribution to sea-level rise  
448 from a new-generation ice-sheet model. *The Cryosphere*, *6*(6), 1561–1576. doi:  
449 10.5194/tc-6-1561-2012
- 450 Gohl, K., Uenzelmann-Neben, G., Larter, R. D., Hillenbrand, C.-D., Hochmuth, K.,  
451 Kalberg, T., . . . Nitsche, F. O. (2013). Seismic stratigraphic record of the  
452 Amundsen Sea Embayment shelf from pre-glacial to recent times: Evidence  
453 for a dynamic West Antarctic ice sheet. *Marine Geology*, *344*, 115–131. doi:  
454 10.1016/j.margeo.2013.06.011
- 455 Golledge, N. R., Fogwill, C. J., Mackintosh, A. N., & Buckley, K. M. (2012). Dy-  
456 namics of the last glacial maximum Antarctic ice-sheet and its response to  
457 ocean forcing. *Proceedings of the National Academy of Sciences*, *109*(40),  
458 16052–16056.

- 459 Graf, W., Oerter, H., Reinwarth, O., Stichler, W., Wilhelms, F., Miller, H., & Mul-  
 460 vaney, R. (2002). Stable-isotope records from Dronning Maud Land, Antarc-  
 461 tica. *Annals of Glaciology*, *35*, 195–201. doi: 10.3189/172756402781816492
- 462 Herman, F., Beaud, F., Champagnac, J.-D., Lemieux, J.-M., & Sternai, P. (2011).  
 463 Glacial hydrology and erosion patterns: A mechanism for carving glacial val-  
 464 leys. *Earth and Planetary Science Letters*, *310*(3-4), 498–508. doi: 10/fxcwgb
- 465 Herman, F., Beyssac, O., Brughelli, M., Lane, S. N., Leprince, S., Adatte, T., ...  
 466 Cox, S. C. (2015). Erosion by an Alpine glacier. *Science*, *350*(6257), 193–195.
- 467 Humphrey, N. F., & Raymond, C. F. (1994). Hydrology, erosion and sediment pro-  
 468 duction in a surging glacier: Variegated Glacier, Alaska, 1982–83. *Journal of*  
 469 *Glaciology*, *40*(136), 539–552. doi: 10.3189/S0022143000012429
- 470 Koppes, M., Hallet, B., Rignot, E., Mouginot, J., Wellner, J. S., & Boldt, K. (2015).  
 471 Observed latitudinal variations in erosion as a function of glacier dynamics.  
 472 *Nature*, *526*(7571), 100–103. doi: 10.1038/nature15385
- 473 Kristoffersen, Y., Hofstede, C., Diez, A., Blenkner, R., Lambrecht, A., Mayer, C.,  
 474 & Eisen, O. (2014). Reassembling Gondwana: A new high quality constraint  
 475 from vibroseis exploration of the sub-ice shelf geology of the East Antarctic  
 476 continental margin. *Journal of Geophysical Research: Solid Earth*, *119*(12),  
 477 9171–9182. doi: 10.1002/2014JB011479
- 478 Kulp, S. A., & Strauss, B. H. (2019). New elevation data triple estimates of global  
 479 vulnerability to sea-level rise and coastal flooding. *Nature Communications*,  
 480 *10*(1), 4844. doi: <https://doi.org/10.1038/s41467-019-12808-z>
- 481 Lambeck, K., Rouby, H., Purcell, A., Sun, Y., & Sambridge, M. (2014). Sea level  
 482 and global ice volumes from the Last Glacial Maximum to the Holocene. *Pro-*  
 483 *ceedings of the National Academy of Sciences*, *111*(43), 15296–15303. doi: 10  
 484 .1073/pnas.1411762111
- 485 Lenaerts, J. T., Brown, J., Van Den Broeke, M. R., Matsuoka, K., Drews, R., Cal-  
 486 lens, D., ... Van Lipzig, N. P. (2014). High variability of climate and surface  
 487 mass balance induced by Antarctic ice rises. *Journal of Glaciology*, *60*(224),  
 488 1101–1110. doi: 10.3189/2014JoG14J040
- 489 MacAyeal, D. R. (1993). A tutorial on the use of control methods in ice-  
 490 sheet modeling. *Journal of Glaciology*, *39*(131), 91–98. doi: 10.3189/  
 491 S0022143000015744
- 492 MacGregor, J. A., Fahnestock, M. A., Catania, G. A., Aschwanden, A., Clow, G. D.,  
 493 Colgan, W. T., ... Seroussi, H. (2016). A synthesis of the basal thermal state  
 494 of the Greenland Ice Sheet. *Journal of Geophysical Research: Earth Surface*,  
 495 *121*(7), 1328–1350. doi: 10.1002/2015JF003803
- 496 Malinen, M., Ruokolainen, J., Råback, P., Thies, J., & Zwinger, T. (2013). Par-  
 497 allel Block Preconditioning by Using the Solver of Elmer. In P. Manninen  
 498 & P. Öster (Eds.), *Applied Parallel and Scientific Computing* (pp. 545–547).  
 499 Berlin, Heidelberg: Springer Berlin Heidelberg.
- 500 Martos, Y. M., Catalán, M., Jordan, T. A., Golynsky, A., Golynsky, D., Eagles, G.,  
 501 & Vaughan, D. G. (2017). Heat Flux Distribution of Antarctica Unveiled. *Geo-*  
 502 *physical Research Letters*, *44*(22), 11,417–11,426. doi: 10.1002/2017GL075609
- 503 Martín-Español, A., King, M. A., Zammit-Mangion, A., Andrews, S. B., Moore, P.,  
 504 & Bamber, J. L. (2016). An assessment of forward and inverse GIA solu-  
 505 tions for Antarctica. *Journal of Geophysical Research: Solid Earth*, *121*(9),  
 506 6947–6965. doi: 10.1002/2016JB013154
- 507 Oerlemans, J. (2002). On glacial inception and orography. *Inception: Mech-*  
 508 *anisms, patterns and timing of ice sheet inception*, *95-96*, 5–10. doi: 10.1016/  
 509 S1040-6182(02)00022-8
- 510 Pachauri, R. K., Allen, M. R., Barros, V. R., Broome, J., Cramer, W., Christ, R.,  
 511 ... others (2014). *Climate change 2014: synthesis report. Contribution of*  
 512 *Working Groups I, II and III to the fifth assessment report of the Intergovern-*  
 513 *mental Panel on Climate Change*. Ipcc.

- 514 Pattyn, F., & Durand, G. (2013). Why marine ice sheet model predictions may di-  
 515 verge in estimating future sea level rise. *Geophysical Research Letters*, *40*(16),  
 516 4316–4320. doi: 10.1002/grl.50824
- 517 Pollard, D., Chang, W., Haran, M., Applegate, P., & DeConto, R. (2016). Large  
 518 ensemble modeling of the last deglacial retreat of the West Antarctic Ice Sheet:  
 519 comparison of simple and advanced statistical techniques. *Geosci. Model Dev.*,  
 520 *9*(5), 1697–1723. doi: 10.5194/gmd-9-1697-2016
- 521 Pollard, D., & DeConto, R. M. (2009). Modelling West Antarctic ice sheet growth  
 522 and collapse through the past five million years. *Nature*, *458*(7236), 329–332.  
 523 doi: 10.1038/nature07809
- 524 Rignot, E., Mouginot, J., & Scheuchl, B. (2011). Ice Flow of the Antarctic Ice Sheet.  
 525 *Science*, *333*(6048), 1427–1430. doi: 10.1126/science.1208336
- 526 Ritz, C., Rommelaere, V., & Dumas, C. (2001). Modeling the evolution of Antarc-  
 527 tic ice sheet over the last 420,000 years: Implications for altitude changes in  
 528 the Vostok region. *Journal of Geophysical Research: Atmospheres*, *106*(D23),  
 529 31943–31964. doi: 10.1029/2001JD900232
- 530 Rückamp, M., Falk, U., Frieler, K., Lange, S., & Humbert, A. (2018). The effect  
 531 of overshooting 1.5 °C global warming on the mass loss of the Greenland ice  
 532 sheet. *Earth Syst. Dynam.*, *9*(4), 1169–1189. doi: 10.5194/esd-9-1169-2018
- 533 Schannwell, C. (2019). *Elmer/Ice simulation files for LGM simulations in*  
 534 *”Glacial cycle ice-sheet evolution controlled by ocean bed properties”*. Zen-  
 535 odo. Retrieved from <https://doi.org/10.5281/zenodo.3564168> doi:  
 536 10.5281/zenodo.3564168
- 537 Schannwell, C., Drews, R., Ehlers, T. A., Eisen, O., Mayer, C., & Gillet-Chaulet,  
 538 F. (2019). Kinematic response of ice-rise divides to changes in ocean  
 539 and atmosphere forcing. *The Cryosphere*, *13*(10), 2673–2691. doi:  
 540 10.5194/tc-13-2673-2019
- 541 Schoof, C. (2007). Ice sheet grounding line dynamics: Steady states, sta-  
 542 bility, and hysteresis. *Journal of Geophysical Research*, *112*(F3). doi:  
 543 10.1029/2006JF000664
- 544 Seddik, H., Greve, R., Zwinger, T., Gillet-Chaulet, F., & Gagliardini, O. (2012).  
 545 Simulations of the Greenland ice sheet 100 years into the future with the  
 546 full Stokes model Elmer/Ice. *Journal of Glaciology*, *58*(209), 427–440. doi:  
 547 10.3189/2012JoG11J177
- 548 Simms, A. R., Lisiecki, L., Gebbie, G., Whitehouse, P. L., & Clark, J. F. (2019).  
 549 Balancing the last glacial maximum (LGM) sea-level budget. *Quaternary*  
 550 *Science Reviews*, *205*, 143–153. doi: 10.1016/j.quascirev.2018.12.018
- 551 Smith, E. C., Hattermann, T., Kuhn, G., Gaedicke, C., Berger, S., Drews, R., ...  
 552 Eisen, O. (2019). Detailed seismic bathymetry beneath ekstroem ice shelf,  
 553 antarctica: Implications for glacial history and ice-ocean interaction. *Earth and*  
 554 *Space Science Open Archive*. doi: 10.1002/essoar.10501125.1
- 555 Spagnolo, M., Phillips, E., Piotrowski, J. A., Rea, B. R., Clark, C. D., Stokes,  
 556 C. R., ... Szuman, I. (2016). Ice stream motion facilitated by a shallow-  
 557 deforming and accreting bed. *Nature Communications*, *7*(1), 10723. doi:  
 558 10.1038/ncomms10723
- 559 Tsai, V. C., Stewart, A. L., & Thompson, A. F. (2015). Marine ice-sheet profiles  
 560 and stability under coulomb basal conditions. *Journal of Glaciology*, *61*(226),  
 561 205–215. doi: 10.3189/2015JoG14J221
- 562 Whitehouse, P. L., Bentley, M. J., & Le Brocq, A. M. (2012). A deglacial model  
 563 for Antarctica: geological constraints and glaciological modelling as a basis for  
 564 a new model of Antarctic glacial isostatic adjustment. *Quaternary Science*  
 565 *Reviews*, *32*, 1–24. doi: 10.1016/j.quascirev.2011.11.016
- 566 Whitehouse, P. L., Gomez, N., King, M. A., & Wiens, D. A. (2019). Solid Earth  
 567 change and the evolution of the Antarctic Ice Sheet. *Nature Communications*,  
 568 *10*(1), 503. doi: 10.1038/s41467-018-08068-y

- 569 Yanites, B. J., & Ehlers, T. A. (2016). Intermittent glacial sliding velocities explain  
570 variations in long-timescale denudation. *Earth and Planetary Science Letters*,  
571 *450*, 52–61. doi: 10.1016/j.epsl.2016.06.022
- 572 Zhao, C., Gladstone, R. M., Warner, R. C., King, M. A., Zwinger, T., & Morlighem,  
573 M. (2018). Basal friction of Fleming Glacier, Antarctica – Part 1: Sensitivity  
574 of inversion to temperature and bedrock uncertainty. *The Cryosphere*, *12*(8),  
575 2637–2652. doi: 10.5194/tc-12-2637-2018